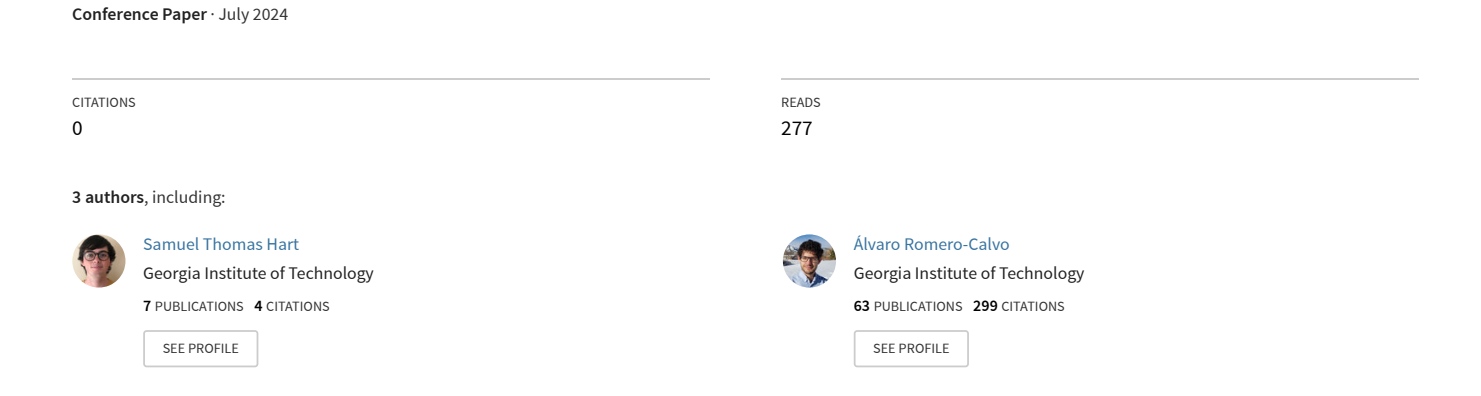
Design and Testing of a Magnetohydrodynamically Pumped Liquid Metal Cooling Loop for CubeSats



Design and Testing of a Magnetohydrodynamically Pumped **Liquid Metal Cooling Loop for CubeSats**

Samuel Hart *, Aaron Robinson †, and Álvaro Romero-Calvo ‡

High-power SmallSats are faced with a limited number of thermal control technologies, many of which are not well suited to a compact form factor or large heat load. This work proposes a new SmallSat heat transfer system composed of a liquid metal cooling loop driven by a magnetohydrodynamic (MHD) pump. The MHD pump leverages the Lorentz force to drive the working fluid without moving parts, which contributes to a low probability of failure. Analytical performance models of the MHD cooling loop are developed and validated against test data collected from a prototype system. Models indicate that the MHD loop is capable of heat transfer rates per unit mass of up to 0.75 W/g in the use case of a 6U CubeSat with a single deployable radiator, exceeding the performance of mechanically pumped fluid loops and thermal straps. Furthermore, a comparison to existing technologies shows that this low-cost system overcomes many of the practical engineering challenges associated with implementing conventional technologies such as heat pipes. This includes improvements in ease of routing, cost of redesign, and the handling of multiple heat sources.

Nomenclature

area of radiator (m²) A_r \boldsymbol{B} magnetic flux density (T) B_r residual flux density (T)

Cflow sensor proportionality constant

 C_p heat capacity (J/K) flow coefficient = diameter of tubing (m)

 D_1 diameter of smaller flow path (m) D_2 = diameter of larger flow path (m)

= Lorentz force (N/m^3) F_{MHD} friction factor

 f_T

gravitational acceleration at sea level, 9.81 m/s² g

height of wetted cross-section between magnets in MHD pump (m) H

Ι = electrical current (A) ID internal diameter = current density (A/m^2) \boldsymbol{J} K = resistance coefficient

 K_1 resistance coefficient of a single 90 degree bend K_c resistance coefficient in a contracting geometry K_e resistance coefficient in an expanding geometry K_{tube} resistance coefficient of a circular loop of tubing

length of tube (m) length of magnet (m)

width of MHD pump electrode in the fluid flow direction (m) l_a

length of pump internal flow passage (m)

^{*}Research assistant, Georgia Institute of Technology Daniel Guggenheim School of Aerospace Engineering, 620 Cherry St. Nw, Atlanta, GA 30332. samuelthart@gatech.edu

[†]Undergraduate research assistant, Morehouse College Physics Department, 830 Westview Dr. Sw, Atlanta, GA 30314

[‡]Assistant professor, Georgia Institute of Technology Daniel Guggenheim School of Aerospace Engineering, 620 Cherry St. Nw, Atlanta, GA 30332. alvaro.romerocalvo@gatech.edu

 m_{Ga} = mass of gallium (kg)

 m_{loop} = mass of MHD cooling loop (kg) m_{MHD} = mass of MHD pump (kg) MHD = magnetohydrodynamic

MPFL = mechanically pumped fluid loop

P = pressure (pa) P_{imperial} = pressure (psi) \dot{Q} = heat transfer rate (W) r = bend radius (m)

 r_{tank} = interior radius of measurement tank (m)

SLA = stereolithography

S = flow sensor output voltage (V)

S.G. = specific gravity

t = thickness of tubing walls (m)

t' = thickness of magnet in magnetization direction (m)

T = temperature (K)

 T_l = temperature of heat load (K) T_r = temperature of radiator (K) \dot{V} = volumetric flow rate (m³/s)

 $\dot{V}_{imperial}$ = volumetric flow rate (US gallons/min)

w =width of wetted cross-section between electrodes in MHD pump (m)

w' = width of magnet (m)

W = power(W)

z = distance along the centroid axis from the surface of the magnet in the magnetization direction (m)

 ϵ_r = emmisivity of radiator μ = dynamic viscosity (pa·s)

 ρ = density (kg/m³)

 $\rho_{\text{Cu}} = \text{density of copper (kg/m}^3)$ $\varrho = \text{electrical resistivity (Ohm·m)}$

 σ = Stefan-Boltzmann constant, 5.670e-8 W/m²/K⁴

I. Introduction

Since their introduction in the 1990s, CubeSats and other small satellites have seen a significant rise in popularity ¹. Their relatively low cost and complexity make them an attractive option for universities, technology demonstrations, and short-timeframe projects. Increasingly, small spacecraft are being used on missions with complex architectures and scientific goals ^{2–4}. As these satellites begin to incorporate more advanced technologies such as electric propulsion and high-data-rate communications, an associated increase in power consumption is expected, and along with it, a need for improved thermal management technologies ⁵.

Due to their small form factor and low power usage, many CubeSat missions rely simply on conductive heat transfer directly from the internal electronics to the spacecraft structure without the use of any additional thermal management hardware. Heat is then radiated into space from the structure of the spacecraft, occasionally with the assistance of high-emissivity coatings ^{6,7}. This architecture is sufficient for low-power systems, but as mission planners begin to design missions using hundreds or thousands of Watts, a more intentional approach to thermal management must be taken ⁸.

Deployable radiators allow for increased rates of heat rejection from the spacecraft, and their use in large spacecraft is well documented ^{5,6,9,10}. The technology has also been considered for implementation on SmallSats with a rollout deployment mechanism ¹¹. This solves one aspect of the thermal management challenge. The remaining problem is transferring heat from within the satellite to the radiator effectively.

Large satellites and spacecraft use thermal straps, heat pipes, and mechanically pumped liquid coolant loops to route heat internally ⁹. Thermal strap technology translates directly to the small satellite architecture, and many commercial examples are available ^{12,13}. A segment of copper is used to conduct heat throughout the spacecraft. The simplicity of the technology is well-suited to this expanding market. However, the heat transfer rates that can be achieved may be insufficient for high-power missions or long transmission distances. Additionally, thermal straps cannot generally be

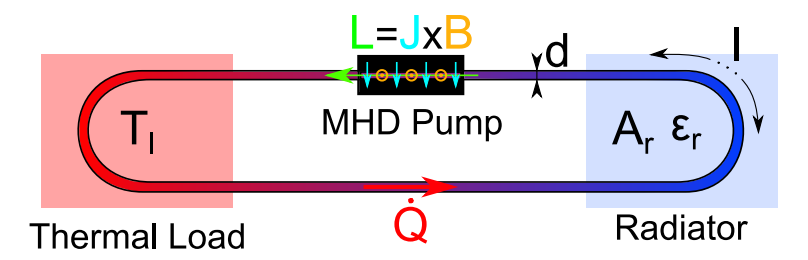


Figure 1 MHD liquid metal cooling loop concept.

actively controlled to vary their heat transfer rate, which can be an issue when different mission phases with varying heat inputs are expected. Thermal switching technology does offer some modulation, but full active control is not feasible ¹⁴.

Heat pipes offer higher heat transfer rates with a slight increase in complexity ⁷. These devices are composed of a metal casing, which contains a capillary wick and an open volume for vapor flow. A saturated liquid-vapor mixture acts as the working fluid within the device. The liquid is vaporized in the hot portion of the heat pipe, and more liquid flows up the capillary wick to replace it. The newly formed vapor flows to the condenser section of the heat pipe, where heat is extracted from the device, and the vapor condenses back into a liquid. This establishes a continuous axial flow within the heat pipe driven by capillary pressure and heat transfer ¹⁵. With appropriate wick design and fluid selection, heat pipes can be capable of transferring hundreds of Watts in a compact form factor ¹⁶. However, they can be challenging to route, expensive, cannot easily be connected to multiple heat sources, and, like thermal straps, cannot generally be actively controlled to maintain tight temperature tolerances ¹⁷. Loop heat pipes have also been developed for small spacecraft and offer >100 W max heat transfer rate, though they are significantly more complex and have less flight heritage than traditional heat pipes ¹⁸. They also suffer from many of the practical complications of a conventional heat pipe when implemented.

Mechanically pumped fluid loops (MPFLs) promise much higher heat transfer rates, can be actively controlled, can be connected to multiple heat sources and radiators, allow simplified routing, and have spaceflight heritage ^{19,20}. The primary issues associated with this technology are mass and volume ⁷. Additionally, mechanical pumps have a high risk of failure due to their internal mechanisms, and as such, systems must implement multiple backup pumps should the primary pump fail. This leads to a mass and volume generally incompatible with the CubeSat form factor, though there are miniature MPFL technologies in development that promise a smaller footprint ²¹. However, even the mini-MPFL is expected to have a pump mass of at least 100 g, excluding electronics, tubing, and the working fluid ²⁰.

Electromagnetic pumps offer a highly reliable alternative to mechanical devices. These pumps operate on the principle that a current-carrying conductor experiences a force when placed perpendicular to a magnetic field. This allows the pump to drive a conducting fluid without the use of moving parts, which proves beneficial in many applications. Annular linear induction pumps (ALIPs) are used in systems containing high-temperature fluids that render mechanical pumps infeasible, such as nuclear devices and concentrated solar energy systems 22,23. These devices are relatively complex in their operation and rely upon a 3-phase AC power supply and a series of copper windings to generate a linearly moving magnetic field along the body of the pump. The varying magnetic field results in an induced current within the fluid, which interacts with the magnetic field to propel the liquid 24. Lower temperature applications that allow for direct contact between electrodes and the working fluid often opt for the simpler magnetohydrodynamic (MHD) pump. In an MHD pump, a static magnetic field is applied to a conductive fluid using either permanent or electric magnets. A DC electrical current is then applied through the fluid perpendicular to the magnetic field, propelling the working fluid through the pump. These devices have seen use in applications ranging from low-noise naval propulsion systems ²⁵ to nanofluidics ²⁶. The simplicity of the device leads to a compact, reliable, and effective pumping system. Additionally, MHD pumps are well suited to work with high thermal conductivity and heat capacity liquids such as mercury, gallium, and other liquid metals, which can be used to efficiently transfer heat²⁷. Furthermore, appropriate applications of magnetic fields and electrical currents can be used to promote mixing and increase heat transfer rates in a liquid metal cooling loop²⁸. The combination of these features makes an MHD pump an attractive option for powering a cooling loop in small spacecraft, as depicted in Figure 1, and while large electromagnetic pumps have been proposed for use in nuclear reactors in space ²⁹, no small-scale MHD device has ever been conceived for low-temperature heat transfer applications outside of Earth's atmosphere.

This paper introduces a small satellite cooling loop using liquid metals and an MHD pump. First, analytical models of the system are developed in Section II.A and II.B to analyze the expected performance. These models are used

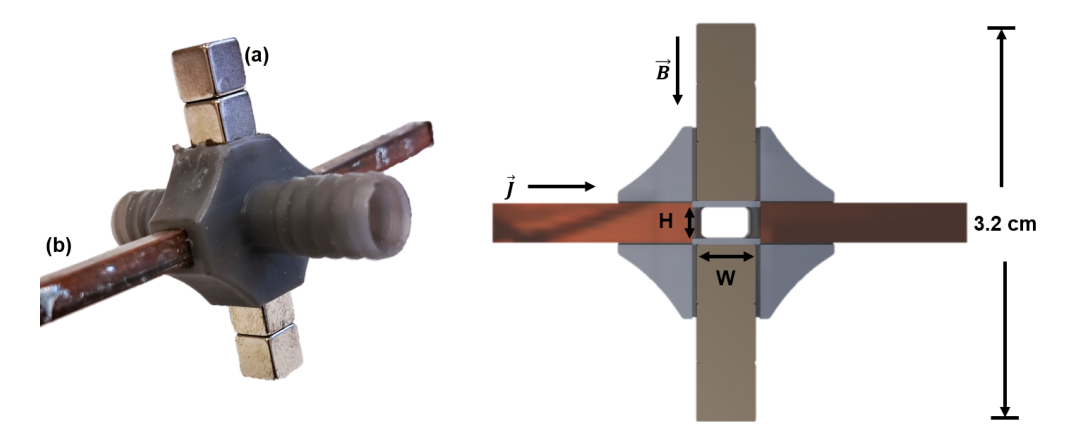


Figure 2 Magnetohydrodynamic pump prototype. (a) N52 neodymium magnet. (b) Copper electrode.

in trade studies in Section III.A and III.B. Hardware tests of a prototype pump using gallium as a working fluid are described in Section II.C, and results are discussed in Section III.C.

II. Materials and Methods

A. Analytical Modeling

The MHD cooling loop is composed of a pump that propels a liquid metal through tubing connecting heat sources within a spacecraft with external radiators. The MHD pump is driven by the Lorentz force,

$$F_{\text{MHD}} = J \times B. \tag{1}$$

where F_{MHD} is the force applied to the working fluid per unit volume, J is the current density, and B is the magnetic flux density. This volumetric force is exerted on the liquid metal by placing permanent magnets perpendicular to electrodes, which conduct an electrical current through the fluid, as shown in Figure 2. The pressure differential provided by the pump is, in first-order approximation,

$$\Delta P = \frac{IB}{H},\tag{2}$$

with dimensions defined in Figure 2 and I and H being the applied current and the height of the wetted pump cross-section, respectively. This model assumes uniform and perpendicular magnetic flux density and current density and that all pressure gains are realized in the rectangular cross-section between the magnets and electrodes.

The magnetic flux density varies with the distance between the sets of permanent magnets on either side of the pump depicted in Figure 2. To estimate this variation, the magnetic flux density along the symmetry axis of a rectangular block magnet can be calculated as ³⁰

$$B = \frac{B_r}{\pi} \left\{ \tan^{-1} \left[\frac{l'w'}{\sqrt{4z^2 + l'^2 + w'^2}} \right] - \tan^{-1} \left[\frac{l'w'}{2(t'+z)\sqrt{4(t'+z)^2 + l'^2 + w'^2}} \right] \right\},\tag{3}$$

where B_r , l', and w' are the residual flux density, length, and width of the magnet, t' is the thickness in the magnetization direction, and z is the distance along the centroid axis from the surface of the magnet. With this relation and Equation 2, the pump output pressure can be estimated. The magnetic flux density is assumed to be uniform and equivalent to the value calculated by Equation 3 at the midpoint between the two sets of permanent magnets in this estimation.

To estimate the flow rate through the cooling loop, the flow resistance must be calculated. The flow coefficient of a fluid component is defined as the number of gallons of water at 60°F that can pass through a component in one minute with a one pound per square inch pressure drop. For a given flow rate and pressure drop, it can be calculated as

$$C_{\nu} = \dot{V}_{\text{imperial}} \sqrt{\frac{S.G.}{\Delta P_{\text{imperial}}}},$$
 (4)

where $\dot{V}_{\rm imperial}$ is the volumetric flow rate in US gallons per minute, S.G. is the specific gravity of the fluid, and $\Delta P_{\rm imperial}$ is the pressure drop through the component in pounds per square inch. The total pressure loss through the pump geometry has contributions from the flow through the narrow rectangular pump geometry as well as losses due to the expanding and contracting flow sections at the outlet and inlet of the pump. The pressure loss due to the uniform rectangular geometry of the pump can be calculated from Darcy's formula and the definition of hydraulic diameter as 31

$$\Delta P = \frac{8\mu(w+H)^2 l_p \dot{V}}{w^3 H^3},\tag{5}$$

with μ , w, l_p , and \dot{V} being the dynamic viscosity, width of the pump cross-section, length of the internal flow path within the pump, and volumetric flow rate, respectively. The losses due to expansion and contraction are calculated as ³¹

$$\Delta P = \frac{\rho K v^2}{2},\tag{6}$$

where ρ is the fluid density, K is the resistance coefficient, and v is the mean flow velocity. For expanding flows, ³¹

$$K_e = \left(1 - \frac{D_1^2}{D_2^2}\right)^2,\tag{7}$$

with D_1 and D_2 being the hydraulic diameters of the smaller and larger flow paths, respectively. For contracting flows, the resistance coefficient is defined as 31

$$K_c = 0.5 \left(1 - \frac{D_1^2}{D_2^2} \right). (8)$$

By combining Equations 4-8, the flow coefficient of the MHD pump and its associated pressure losses can be computed. The losses through the tubing, assuming it forms a single circular loop, are estimated using Equation 6, with

$$K_{\text{tube}} = 3\left(0.25 f_T \pi \frac{r}{d} + 0.5 K_1\right) + K_1,$$
 (9)

where f_T is the friction factor, r/d is the bend radius of the tubing divided by its inner diameter, and K_1 is the resistance coefficient of a single 90 degree bend with equivalent bend radius³¹. By setting the pressure developed by the pump equivalent to the pressure losses incurred in the fluid flow path and solving the equation numerically, the flow rate can be estimated. The maximum heat transfer rate achievable by the cooling loop can then be computed as

$$\dot{Q} = \rho C_n \dot{V} \Delta T \tag{10}$$

where C_p is the heat capacity of the liquid metal and $\Delta T = T_l - T_r$ is the temperature differential between the heat load and radiator.

B. Simplified Model

A simplified model of the pump flow rate and cooling loop performance is developed for use in trade studies and to gain an intuitive understanding of the factors affecting the system. At low flow rates, the liquid metal moves inside the tube adopting a laminar flow regime (Re < 2300). The liquid volumetric flow rate can be related to the pressure drop through the loop by the Hagen-Poiseuille law³²

$$\dot{V} = \frac{\pi d^4 \Delta P}{128\mu l},\tag{11}$$

where *l* and *d* are the length and internal diameter of the tube, respectively. This relation assumes that head losses due to flow through the pump itself are negligible and that the cooling loop can be represented as a single straight section of tubing. If the pump is paired with an external radiator, as shown in Figure 1, the radiator stabilizes at the equilibrium temperature

$$T_r = \left(\frac{\dot{Q}}{\sigma A_r \epsilon_r}\right)^{1/4},\tag{12}$$

Table 1 Thermophysical properties of candidate liquid metals at 25°C and 1 atm.

| Liquid | Density [kg/m ³] | Viscosity [Pa·s/10 ⁻³] | Spec. Heat [J/Kg/K] | Therm. Cond. [W/m/K] | Fus. Temp. [°C] | Resistivity [m·Ohm/10 ⁻⁷] |
|-----------|---------------------------------|---------------------------------------|------------------------|----------------------|-----------------|---------------------------------------|
| NaK-77 | 866 | 0.94 | 982 | 22.4 | -12.6 | 5 |
| Gallium | 6095 | 1.969 | 370 | 30.2 | 30 | 1.4 |
| Galinstan | 6440 | 2.4 | 296 | 16.5 | -19 | 2.9 |
| Mercury | 13534 | 1.5 | 139 | 8.3 | -38.9 | 9.61 |

with σ being the Stefan-Boltzmann constant, and A_r and ϵ_r being the surface area and emissivity of the radiator, respectively. Because it is connected to a heat load at a constant temperature, T_l , a physical limit is imposed on the amount of heat that can be emitted by the radiator. The heat transported by the loop can be determined by solving the algebraic equation

$$\dot{Q} = \rho C_p \dot{V} \Delta T = \frac{\pi \rho C_p d^4 IB}{128 \mu l H} \left[T_l - \left(\frac{\dot{Q}}{\sigma A_r \epsilon_r} \right)^{1/4} \right]. \tag{13}$$

The mass of the MHD loop is calculated as

$$m_{\text{loop}} = \frac{\pi \rho l d^2}{4} + \pi \rho_{\text{Cu}} lt(t+d) + m_{\text{MHD}}, \tag{14}$$

where, from left to right, the mass of the liquid metal inside the tube, the tube, and the MHD pump have been considered. The mass of the MHD pump, m_{MHD} , is 11 g based on measurements of the prototype pump.

Finally, the power W consumed by the system is computed as the addition of ohmic losses that arise due to electrical current flowing through the working fluid and the work devoted to moving the liquid and compensating for viscous drag. The result is

$$W = \left[\frac{\varrho w}{H l_a} + \frac{\pi d^4 B^2}{128\mu l H^2} \right] I^2, \tag{15}$$

with ϱ being the electrical resistivity of the conducting liquid and l_a being the width of the electrode in the fluid flow direction. Losses due to current flow through the electrodes are ignored. At this point, a few important remarks should be made regarding equations 13–15:

- 1) The width of the MHD pump electrode, l_a , does not influence the heat transferred by the system under the assumption of an adiabatic wall and has only a minor effect on power consumption, but it determines $m_{\rm MHD}$. In other words, pumps with a short length in the flow direction are beneficial for this application.
- 2) Pump power consumption is well below 1 W in most scenarios of interest.
- 3) Heat transport is strongly influenced by the area of the radiator: the larger A_r , the lower the radiator temperature and the higher the heat transferred by the loop. However, the liquid metals listed in Table 1 melt at temperatures between -38.9°C and 30°C. The operational point of the system must be selected to prevent the liquid from freezing and guarantee system restart. Alternatively, a heater can be added to the system to melt the working fluid.

C. Experimental Setup

A prototype pump is constructed from an additively manufactured plastic frame which is SLA printed using a Formlabs Form 3B with Gray V4 resin as shown in Figure 2. Three 4.76 mm cubic nickel-plated N52 neodymium magnets* are inserted into either side of the frame with a separation distance of 3.5 mm. Copper electrodes with a 3.18 mm square cross-section[†] are placed perpendicular to the magnets with 5.5 mm between them. These electrodes remain in direct contact with the working fluid. The pump has a 2.5 mm by 4.0 mm rectangular wetted cross-section with the shorter dimension being between the magnets. Hose barbs are designed into the pump to allow it to interface with 4.76 mm inner diameter (ID) flexible PVC tubing[‡]. Gallium[§], with a purity of 99.99 %, is used as the working fluid. The

^{*}PN: B333-N52, procured from K&J Magnetics, Inc.

[†]PN: 89985K417, procured from McMaster-Carr

[‡]PN: 5233K53, procured from McMaster-Carr

[§]ASIN: B07SLB57P6, procured from Amazon.com



Figure 3 Experimental setups used to determine MHD pump performance characteristics.

pump undergoes two test series to characterize its performance, one measuring the static pressure gain and the other measuring the flow rate achieved in a prototype cooling loop. A Keysight E36233A DC power supply is used in both test series.

1. Pressure Tests

The pump is attached between two 2.54 cm inner diameter SLA printed cylindrical tanks partially filled with gallium; one is placed on a scale, as shown in Figure 3(a). When current is applied to the electrodes, gallium is pumped from the base of one tank to the other. This continues until equilibrium is reached between the pressure output of the pump and the hydrostatic pressure difference between the two tanks. The change in mass of one of the two tanks is then recorded. The applied current is then increased by one ampere, the tanks are again allowed to come to equilibrium, and the mass is recorded again. This is repeated for a range of 1 to 15 amperes. The process is then repeated starting at 15 amperes and decreasing in 1 ampere increments. This repetition is done to account for the effects of an advancing or receding contact line between the gallium and the tank walls, which may affect the mass of gallium within the tank. The pressure applied by the pump is then calculated by the hydrostatic pressure rise determined from the recorded masses as

$$P = \frac{2gm_{\text{Ga}}}{\pi r_{\text{tank}}^2},\tag{16}$$

Pump

where g is the acceleration due to gravity, m_{Ga} is the mass increase of gallium in one tank, and r_{tank} is the interior radius of the cylindrical tank.

2. Flow Rate Tests

Flow rate tests are conducted using a single MHD pump connected to a magnetic flow rate sensor with the same geometry as the pump by two 15 cm sections of 4.76 mm inner diameter flexible PVC tubing, as shown in Figure 3(b). The sensor operates based on Farraday's law of induction and produces a voltage proportional to the volumetric flow rate 33

$$S = C\dot{V},\tag{17}$$

with C being a proportionality constant related to the magnetic flux density, working fluid, and geometry within the sensor. The value of C is determined to be 1.8×10^{-4} V/ml/s. The output voltage is amplified by a factor of 1001 and measured by a LabJack T7 data acquisition system with an LJTick-InAmp amplifier. Magnets identical to those used in the pump are used to generate a magnetic field within the sensor flow cross-section. This measurement device is chosen to avoid material compatibility issues that arise when gallium is passed through many commercially available sensors. The proportionality constant, C, of the sensor is first determined by flowing gallium through it at a measured flow rate using a peristaltic pump. This is repeated at multiple flow rates. The linear coefficient relating voltage to flow rate is the slope of a line fit to the calibration data with intercept at the origin.

Table 2 Geometric and physical properties of MHD loop in simulation.

| Parameter | Value | Description | | | | |
|--------------|--------------------|--|--|--|--|--|
| l | 0.6 m | Length of cooling loop | | | | |
| d | 4.76 mm | Internal diameter of tubing | | | | |
| B | 0.65 T | Magnetic flux density in pump (approximated to be uniform) | | | | |
| l_a | 3.18 mm | Length of MHD pump acceleration volume | | | | |
| A_r | 0.12 m^2 | Surface area of radiator | | | | |
| ϵ_r | 0.9 | Emissivity of radiator | | | | |
| T_l | 333 K | Temperature of heat load | | | | |
| H | 2.5 mm | Length of pump flow cross-section between magnets | | | | |
| w | 4.0 mm | Width of pump flow cross-section between electrodes | | | | |
| I | 1 A | Current passed through electrodes | | | | |
| t | 0.635 mm | Thickness of copper tubing walls | | | | |

An electrical current is applied to the pump, and the fluid flow rate is allowed to stabilize. The voltage output from the flow sensor is then recorded. This process is repeated at multiple input currents ranging from 1 to 15 A.

III. Results and Discussion

A. Comparison of Working Fluids

Figure 4 shows the analytical prediction of the heat transferred by an MHD cooling loop containing each of the liquids listed in Table 1 as well as a copper heat strap as a function of the overall mass of the device. These predictions are based on the assumptions and equations developed in Section II.B for a setup shown in Figure 1. The physical properties of the cooling loop and radiator are listed in Table 2. These values are selected to reflect heat transport across the full length of a 6U CubeSat with a single $20 \text{ cm} \times 30 \text{ cm}$ deployable radiator.

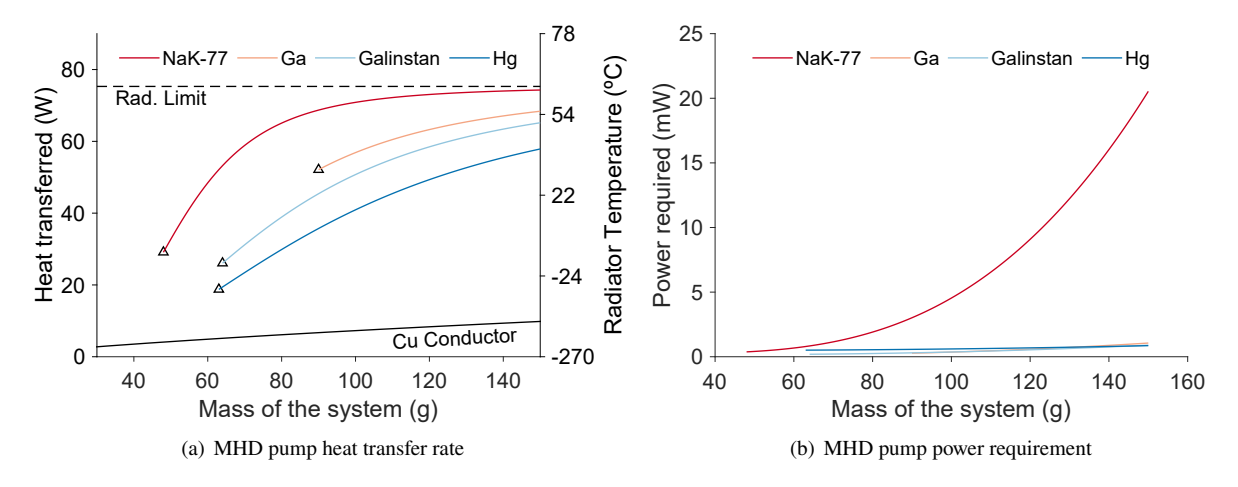


Figure 4 Heat transferred and power required by the cooling loop as a function of its mass m for different candidate liquids operating at 1 Amp.

NaK-77 is capable of transferring more heat per unit mass than any other liquid metal in the MHD loop thanks to its higher specific heat and lower density. However, it is also the most dangerous due to its high reactivity with water, and it requires more power owing to its low density ³⁴. Mercury offers the widest operating temperature range

at the expense of performance, while Galinstan and Gallium lie in between. Gallium has the narrowest operating temperature range and is better suited for very high-power applications; however, it is the safest to handle and relatively inexpensive ³⁵. All of the candidate MHD loops outperform heat straps in this operating range. A direct comparison with heat pipes is complicated by the highly design and temperature-dependent performance of such systems and is therefore excluded ^{17,19,36}. It should be noted, however, that heat pipes are capable of significant heat transfer rates, with aluminum-cased ammonia systems being a primary example. These devices are not generally limited by their heat transfer rate, but by the shortcomings which will be discussed in Section III.D.

While a thin-walled copper tube is used to route the gallium in this trade study, other materials, including flexible plastics such as PEEK, can be used ^{21,37}. Flexible materials may prove beneficial when installing the system into a spacecraft. Copper is attractive primarily due to its material compatibility and thermal conductivity ³⁸.

B. Geometry Optimization

As the pump geometry affects not only the flow resistance of the pump but also the magnetic flux density within it, a trade space exists. Narrower flow passages contribute to both larger magnetic flux densities and pump output pressures while also increasing viscous losses in the flow. To elucidate theses effects, contours of the pump flow coefficient and static output pressure are developed in Figure 5 based on the equations derived in Section II.A.

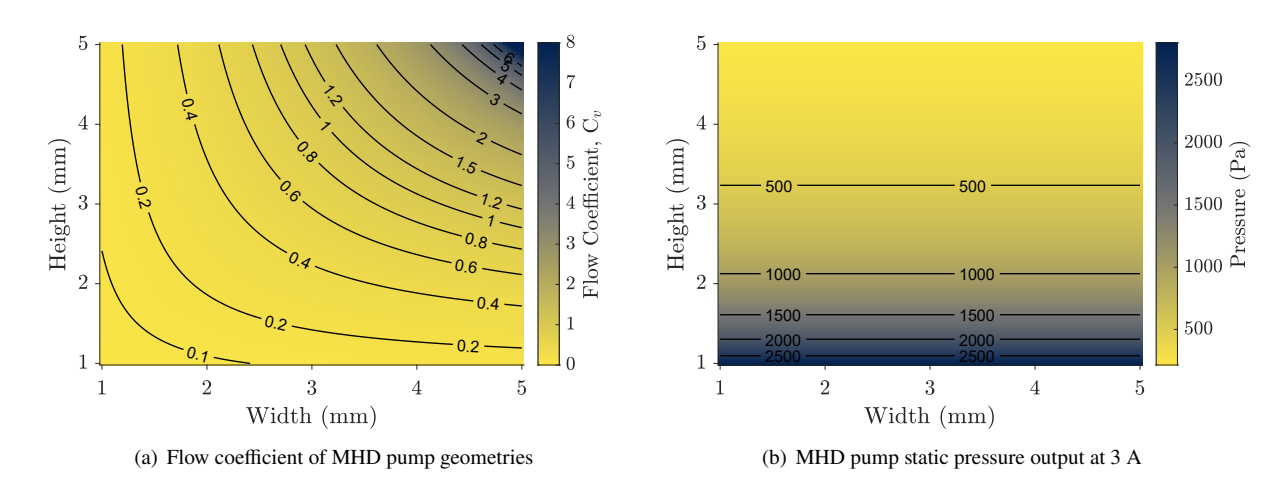


Figure 5 MHD pump geometry optimization curves.

It is evident from Figure 5 that the ideal pump with regard to flow rate would have a large width (distance between the pump electrodes). This increases the flow coefficient and has only a minor negative impact on power consumption based on Equation 15. It would require that larger magnets be used to maintain a magnetic field across the entire cross-section, which would result in a significant increase in mass and should be considered. The ideal pump height cannot be readily determined. The greatest output pressure is attained by a pump with a small height, but this simultaneously decreases the flow coefficient. The optimal height depends on the overall flow resistance of the system as well as the electrical current applied to the electrodes.

C. Hardware Tests

The pressure output by the system in a steady non-flowing configuration is evaluated and plotted in Figure 6. The pressure output varies linearly with the applied current, as predicted by the analytical model of the system. The model overpredicts the measured output, likely due to the assumptions adopted in its development, particularly the assumptions of uniform current density and magnetic flux density. Pressure varies as the square root of the applied power as analytical models have predicted. The power required in this test is largely due to the resistance of the electrical leads connecting the pump to the DC power supply. The pump has a resistance of 1.5 ± 0.5 mOhms between its electrodes, meaning it would draw only 22.5 mW at 15 A if power were efficiently transmitted to it. This highlights a key design consideration for this system. The flow path of current between the power processing unit and the pump itself should be minimized to reduce ohmic losses.

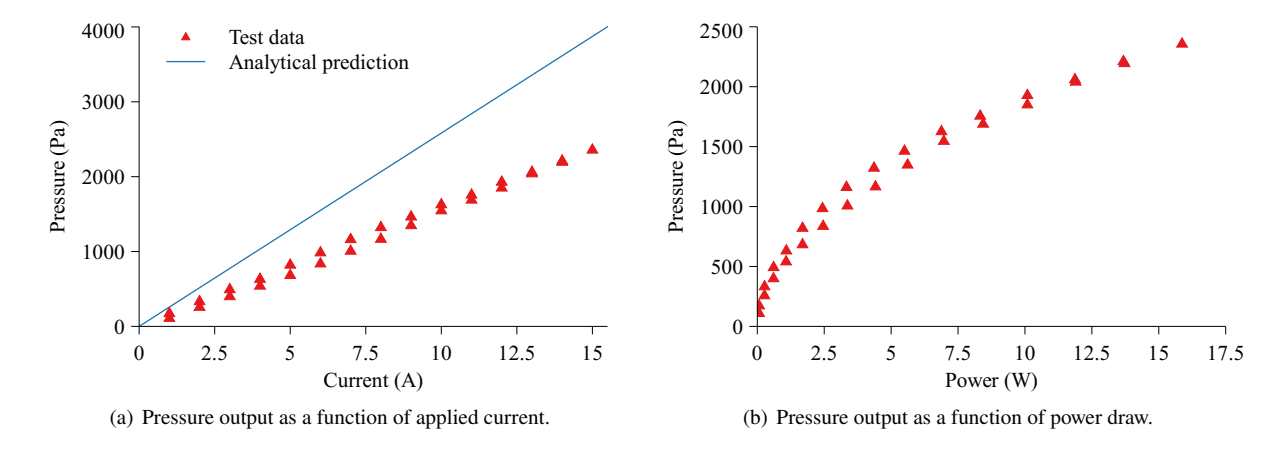


Figure 6 Static pressure rise from MHD pump.

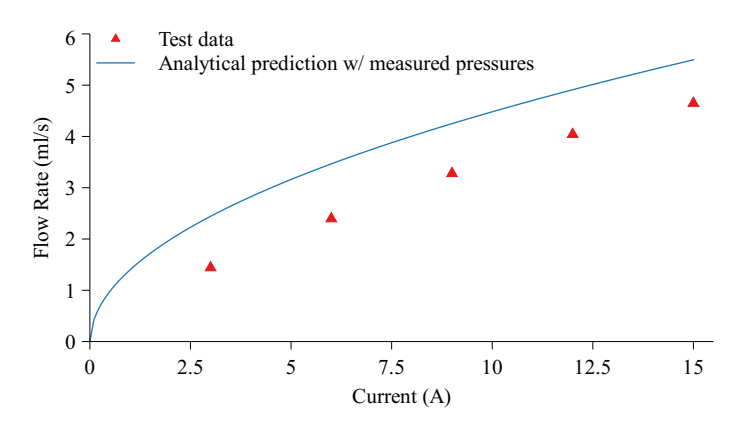


Figure 7 Measured flow rate in a 30 cm loop.

The calculated flow coefficient and flow model developed in Section II.A are validated by plotting estimated flow rates at varied electrical currents against measured data in Figure 7. The pressure inputs to this model are chosen to match experimental data. This figure shows the measured fluid flow rates through a 30 cm loop of 4.76 mm ID tubing with a single MHD pump and a flow rate sensor with internal geometry identical to the pump. The estimates slightly overpredict the flow rate. This could be due to a number of factors including simplifying assumptions made in developing the flow coefficient estimate, mild deformations of the flexible PVC tubing, gallium oxide layers forming and artificially decreasing the diameter of flow passages, and viscosity variations with temperature. Additionally, it is of note that the sensor itself accounts for roughly 30% of the viscous losses in the loop according to analytical estimations, so a considerably higher flow rate would be expected in a loop containing only a pump and tubing.

The simple model developed in Section II.B shows poorer agreement with the test data. The measured flow rates are approximately one order of magnitude smaller than those predicted by the simple model. This is largely because it does not account for head pressure losses due to flow through the flow rate sensor or the pump itself. The internal geometry of these components represents the narrowest flow passage in the cooling loop. Furthermore, the disruptions to the flow at the interface between the pump and the tubing contribute to additional losses.

There are a number of possible improvements to the MHD cooling loop. The performance of the pump is directly related to the magnetic flux density and electrical current density that exist within it. The electrical current density can be easily increased, with the spacecraft power system being the primary limiting factor in the design. Currents upward of 1 A are not always available, especially on CubeSats. As such, the implementation of a DC-DC converter capable of accepting a low-current input and developing a high-current low-voltage output would increase the capabilities of the MHD-pumped cooling loop onboard a small spacecraft. The performance of the pump could further be improved by augmentations to the permanent magnets. The addition of an iron yoke joining the two sets of magnets could minorly increase the average magnetic flux density within the pump³⁹. The use of larger magnets could have a similar effect.

Table 3 Comparison of heat transfer technologies in a 6U CubeSat with an 80 W heat load being transported 30 cm to a 20 cm \times 30 cm deployable radiator.

| Technology | $\frac{\dot{Q}}{m}$ | Active Control | # Hot Spots | Reliability | Ease of Routing | Redesign Cost | Cost | Heritage |
|---------------------------------|---------------------|-------------------|----------------|-------------|-----------------|------------------|------|----------|
| Thermal straps | Low | No | Med. | High | Med. | Low | Low | High |
| Heat pipes | High | No | Low | High | Low | Med. | Med. | High |
| Loop heat pipes | High | No | Low | Med. | Low | High | High | Med. |
| Mechanically pumped fluid loops | Med. | Yes | High | Low | High | Low | High | Med. |
| MHD cooling loop | High | Yes | High | High | High | Low | Med. | Low |

Further performance gains can be realized by placing multiple pumps in the same cooling loop. By placing two pumps in series both electrically and in the fluid system, the pressure gain is doubled. This comes at the expense of doubling the ohmic losses of the system, though this is not a substantial amount of power (15 mW for a 10 A current input). An additional benefit of using two pumps is that their magnetic poles can be pointed in opposite directions, thereby reducing the total torque induced on the spacecraft by the presence of permanent magnets in the Earth's magnetic field. It is also possible to use one of the two pumps as a flow rate sensor, which could be beneficial for active control and system health monitoring.

D. Technology Comparison

MHD pumped cooling loops address the same thermal challenges as thermal straps, heat pipes, and MPFLs. Each of these technologies is suited to particular applications. The individual advantages and disadvantages of each are presented in Table 3, with reference to an 80 W heat load that must be transmitted 30 cm to a 20 cm × 30 cm deployable radiator. Thermal straps are a high-reliability solution when small heat fluxes must be transported over short distances, but they perform poorly in the current use case, as indicated in Figure 4(a). Heat pipes and loop heat pipes offer substantially higher heat transfer rates per unit mass ¹⁷. The primary disadvantage of these technologies is that high-performance versions rated for the space environment are expensive, and these technologies can be challenging to route compared to other options ²¹. MPFLs achieve high heat transfer rates per unit mass over both short and long distances - 0.26 W/g for miniature MPFLs and 0.07 W/g for large-scale systems ^{21,40}. These systems are also relatively easy to route, can handle heat loads from multiple locations, and are relatively modular and simple to redesign if minor changes in length are needed ²⁰. However, the pumps have a relatively high probability of failure compared to heat pipes or thermal straps, and the cost of the system is likely to be substantial compared to less complex options ²¹. MHD cooling loops share all of the benefits of a mechanically pumped system, except for flight heritage. Additionally, MHD systems are more reliable due to their lack of moving parts, and they are lighter weight when designed for the heat loads and length scales seen in CubeSats. For these reasons, an MHD pumped liquid metal cooling loop is an attractive option for high-power CubeSats.

IV. Conclusion

Magnetohydrodynamically-pumped cooling loops fill a gap in the SmallSat heat transfer market. Their low mass and volume, coupled with high heat transfer rate, make them well-suited for high-power CubeSats and small satellites. Test data shows that a prototype pump using gallium as a working fluid is capable of a flow rate of 4.6 ml/s using 15 A in a 30 cm cooling loop, which corresponds to a heat transfer rate of up to 10.4 W/K. Additionally, the lack of moving parts increases the reliability of the system. This technology also offers the potential for precise thermal control due to the variable flow rate of the pump. As high-power systems become commonplace in small satellites and CubeSats, technologies like this will become necessary to meet their thermal requirements.

Acknowledgments

This material is based upon work supported by the National Science Foundation Graduate Research Fellowship under Grant No. DGE-2039655. Aaron Robinson acknowledges the support offered by the National Science Foundation under REU grant #2244423. This technology is protected by US Application No. 63/504,558.

References

- [1] Kulu, E., "Nanosatellite Launch Forecasts Track Record and Latest Prediction," *AIAA Small Satellite Conference*, Logan, UT, 2022, pp. 1–17. URL https://digitalcommons.usu.edu/cgi/viewcontent.cgi?article=5166&context=smallsat.
- [2] Bouwmeester, J., and Guo, J., "Survey of worldwide pico- and nanosatellite missions, distributions and subsystem technology," *Acta Astronautica*, Vol. 67, No. 7, 2010, pp. 854–862. https://doi.org/10.1016/j.actaastro.2010.06.004.
- [3] Sternberg, D., Essmiller, J., Colley, C., Klesh, A., and Krajewski, J., "Attitude Control System for the Mars Cube One Spacecraft," 2019 IEEE Aerospace Conference, 2019, pp. 1–10. https://doi.org/10.1109/AERO.2019.8741816.
- [4] Agarwal, R., Oh, B., Fitzpatrick, D., Buynovskiy, A., Lowe, S., Lisy, C., Kriezis, A., Lan, B., Lee, Z., Thomas, A., Wallace, B., Costantino, E., Miner, G., Thayer, J., D'Amico, S., Lemmer, K., Lohmeyer, W., and Palo, S., "Coordinating Development of the SWARM-EX CubeSat Swarm Across Multiple Institutions," *AIAA Small Satellite Conference*, Logan, UT, 2021, pp. 1–12. URL https://digitalcommons.usu.edu/cgi/viewcontent.cgi?article=5104&context=smallsat.
- [5] Hengeveld, D., Moulton, J., Lockyer, S., Taft, B., and Kwas, A., "Enabling High-Power SmallSats with Advanced Thermal Management," AIAA Small Satellite Conference, Logan, UT, 2019. URL https://digitalcommons.usu.edu/smallsat/2019/all2019/ 292.
- [6] Hengeveld, D., Moulton, J., Wilson, M., Taft, B., and Kwas, A., "Thermal Design Considerations for Future High-Power Small Satellites," 48th International Conference on Environmental Systems, Albuquerque, NM, 2018. URL http://hdl.handle.net/2346/74080.
- [7] NASA, "Small Spacecraft Technology State-of-the-Art," Tech. Rep. NASA/TP—2022–0018058, NASA, Ames Research Center, Moffett Field, California, Jan. 2023. URL https://www.nasa.gov/smallsat-institute/sst-soa/.
- [8] Miesner, S., Wolk, K., Furst, B., Daimaru, T., Sunada, E., Roberts, S., Bellardo, J., and Kuo, J., "Thermal Testing of an AMDROHP (Additively Manufactured Deployable Radiator Oscillating Heat Pipes) for Use in High-Powered CubeSats," ASME 2023 International Mechanical Engineering Congress and Exposition, 2024. https://doi.org/10.1115/IMECE2023-114249.
- [9] Gilmore, D., Spacecraft thermal control handbook. 1: Fundamental technologies, 2nd ed., Aerospace Press [u.a.], El Segundo, Calif. 2002.
- [10] Wertz, J. R., Everett, D. F., and Puschell, J. J. (eds.), *Space mission engineering: the new SMAD*, No. v. 28 in Space technology library, Microcosm Press: Sold and distributed worldwide by Microcosm Astronautics Books, Hawthorne, CA, 2011.
- [11] Yendler, B., Meginnis, A., and Reif, A., "Thermal Management for High Power Cubesats," *AIAA Small Satellite Conference*, Logan, UT, 2020. URL https://digitalcommons.usu.edu/smallsat/2020/all2020/41.
- [12] "Thermal Management Technologies Thermal Strap Catalog," Product Catalog, Thermal Management Technologies, Logan, UT, Jan. 2020. URL https://www.tmt-ipe.com/thermal-components.
- [13] "Thermal Straps," Product Catalog SDL/11-224 Rev. F, Space Dynamics Laboratory, Logan, UT, 2024. URL https://www.sdl.usu.edu/downloads/brochures/thermal-straps.pdf.
- [14] Du, T., Xiong, Z., Delgado, L., Liao, W., Peoples, J., Kantharaj, R., Chowdhury, P. R., Marconnet, A., and Ruan, X., "Wide range continuously tunable and fast thermal switching based on compressible graphene composite foams," *Nature Communications*, Vol. 12, No. 1, 2021, p. 4915. https://doi.org/10.1038/s41467-021-25083-8.
- [15] Brouwer, H., Groot, Z., Guo, J., and Gerner, H. J. v., "Solving the Thermal Challenge in Power-Dense CubeSats with Water Heat Pipes," *AIAA Small Satellite Conference*, Logan, UT, 2017. URL https://digitalcommons.usu.edu/smallsat/2017/TS7AdvTech2/4.
- [16] Brennan, P., Kroliczek, E., Jen, H., and McIntosh, R., "Axially grooved heat pipes 1976," *12th Thermophysics Conference*, American Institute of Aeronautics and Astronautics, Albuquerque, NM, 1977. https://doi.org/10.2514/6.1977-747.

- [17] Brennan, P. J., and Kroliczek, E. J., "Heat Pipe Design Handbook: Volume I," Tech. Rep. NASA-CR-163661, NASA, Jun. 1979. URL https://ntrs.nasa.gov/citations/19810065690, nTRS Author Affiliations: B and K Engineering, Inc. NTRS Document ID: 19810065690 NTRS Research Center: Goddard Space Flight Center (GSFC).
- [18] Richard, B., Anderson, W. G., and Crawmer, J., "Development of a 3D Printed Loop Heat Pipe," 2019 35th Semiconductor Thermal Measurement, Modeling and Management Symposium (SEMI-THERM), San Jose, CA, 2019, pp. 58–60. URL https://ieeexplore.ieee.org/document/9165293.
- [19] Thurman, R. L., and McCall, F. C., "Design and Control of Space Station Freedom U.S. Laboratory Active Thermal Control System," SAE Transactions, Vol. 101, 1992, pp. 322–346. https://doi.org/https://doi.org/10.4271/921109.
- [20] van Es, J., Pauw, A., van den Berg, R., and van Kleef, A., "Micro-pumped cooling loop to standardize micro-sat thermal control," 69th International Astronautical Congress, Bremen, Germany, 2018. URL https://iafastro.directory/iac/archive/browse/IAC-18/C2/7/42197/.
- [21] van Es, J., Ganzeboom, T., van den Berg, T. H., Van Vliet, A., Brouwer, H. S. B., and Elvik, S., "Mini Mechanically Pumped Loop Modelling, Design and Tests for standardized cubesat thermal control," 50th International Conference on Environmental Systems, Virtual Event, 2021. URL https://hdl.handle.net/2346/87057.
- [22] Lorenzin, N., and Abánades, A., "A Review on the Application of Liquid Metals as Heat Transfer Fluid in Concentrated Solar Power Technologies," *International Journal of Hydrogen Energy*, Vol. 41, 2016, pp. 6990–6995. https://doi.org/10.1016/j.ijhydene.2016.01.030.
- [23] Geng, S. M., and Reid, T. V., "Two-Step Multi-Physics Analysis of an Annular Linear Induction Pump for Fission Power Systems," 14th International Energy Conversion Engineering Conference, Salt Lake City, UT, 2016. URL https://ntrs.nasa.gov/ citations/20160014541, NTRS Document ID: 20160014541 NTRS Research Center: Glenn Research Center (GRC).
- [24] Sharma, P., Sivakumar, L. S., Prasad, R. R., Saxena, D. K., Kumar, V. A. S., Nashine, B. K., Noushad, I. B., Rajan, K. K., and Kalyanasundaram, P., "Design, Development and Testing of a Large Capacity Annular Linear Induction Pump," *Energy Procedia*, Vol. 7, 2011, pp. 622–629. https://doi.org/10.1016/j.egypro.2011.06.083.
- [25] Nishigaki, K., Sha, C., Takeda, M., Peng, Y., Zhou, K., Yang, A., Suyama, D., Qing, Q. J., Yan, L., Kiyoshi, T., and Wada, H., "Elementary study on superconducting electromagnetic ships with helical insulation wall," *Cryogenics*, Vol. 40, 2000, pp. 353–359. https://doi.org/10.1016/S0011-2275(00)00049-7.
- [26] Al-Habahbeh, O. M., Al-Saqqa, M., Safi, M., and Abo Khater, T., "Review of magnetohydrodynamic pump applications," *Alexandria Engineering Journal*, Vol. 55, No. 2, 2016, pp. 1347–1358. https://doi.org/10.1016/j.aej.2016.03.001.
- [27] Heinzel, A., Hering, W., Konys, J., Marocco, L., Litfin, K., Müller, G., Pacio, J., Schroer, C., Stieglitz, R., Stoppel, L., Weisenburger, A., and Wetzel, T., "Liquid Metals as Efficient High-Temperature Heat-Transport Fluids," *Energy Technology*, Vol. 5, 2017, pp. 1026–1036. https://doi.org/10.1002/ente.201600721.
- [28] Modestov, M., Kolemen, E., Fisher, A. E., and Hvasta, M. G., "Electromagnetic control of heat transport within a rectangular channel filled with flowing liquid metal," *Nuclear Fusion*, Vol. 58, 2018. https://doi.org/10.1088/1741-4326/aa8bf4.
- [29] Maidana, C. O., "Design of Annular Linear Induction Pumps for Space Nuclear Reactors," Thermo-Magnetic Systems for Space Nuclear Reactors: An Introduction, edited by C. O. Maidana, SpringerBriefs in Applied Sciences and Technology, Springer International Publishing, Cham, 2014, pp. 33–47. https://doi.org/10.1007/978-3-319-09030-6_5.
- [30] Patel, H. D., "Use of Permanent Magnets to Improve the Seismic Behavior of Light-Framed Structures," Ph.D. thesis, Virginia Tech, May 2005. URL http://hdl.handle.net/10919/42707.
- [31] Crane Co., Flow of Fluids Through Valves, Fittings, and Pipe, Vervante, 1988.
- [32] Sutera, S. P., and Skalak, R., "The History of Poiseuille's Law," *Annual Review of Fluid Mechanics*, Vol. 25, No. 1, 1993, pp. 1–20. https://doi.org/10.1146/annurev.fl.25.010193.000245.
- [33] Aundal, K. T., "Permanent magnet flowmeter with noncircular sensing passage,", Aug. 2005. URL https://patents.google.com/patent/US6931943B1/en.
- [34] EGO, "Safety Data Sheet Thermostats filled with Potassium-sodium alloy (NaK)," Safety Data V1, EGO, Apr. 2021. URL https://www.gev-online.com/resources/Artikelinfo/ Mzc1MjQ2X1NlY0Rhc2hfNzAxNTNfRU5VX1VOMzU0M19XU0ZSRUk=.pdf.

- [35] Aldrich, "Gallium Safety Data Sheet V6.6," Safety Data Sheet Aldrich 203319, Sigma-Aldrich, Sep. 2021. URL https://www.sigmaaldrich.com/US/en/sds/aldrich/203319.
- [36] Gerner, H. J. v., Brouwer, H., Groot, Z. d., and Guo, J., "Water-filled heat pipes for CubeSat thermal control," *IOP Conference Series: Materials Science and Engineering*, Vol. 1139, No. 1, 2021, p. 012003. https://doi.org/10.1088/1757-899X/1139/1/012003.
- [37] Saba Z. Shaik, Oliver Jia-Richards, and Paulo C. Lozano, "Characterization of a Single-Polarity Electrospray Propulsion System," 37th International Electric Propulsion Conference, Cambridge, MA, 2022. URL https://hdl.handle.net/1721.1/145401.
- [38] McAfee, R., Fish, M., Baker, D., Gess, J., and Boteler, L., "Compatibility Analysis of Liquid Gallium and Common Packaging Metals for Application in Electronic Component Thermal Management," *InterSociety Conference on Thermal and Thermomechanical Phenomena in Electronic Systems, ITHERM*, Vol. 2020-July, 2020, pp. 1276–1281. https://doi.org/10.1109/ ITherm45881.2020.9190557.
- [39] Andreas Urban, "Permanent magnet with yoke for generating a strong magnetic field for educational purposes,", Jul. 2009. URL https://patents.google.com/patent/DE202009005692U1/en, number: DE202009005692U1.
- [40] Benthem, R. C. v., van Gerner, H. J., Es, J. v., Vliet, A. v., Put, P. v., Elst, J., and Schwaller, D., "Valve-less Mechanically Pumped Fluid Loop (MPFL) using East and West Panels of a Large Telecommunication Satellite as Radiator," 45th International Conference on Environmental Systems, Bellevue, WA, 2015. URL http://hdl.handle.net/2346/64354.